



HAL
open science

High rate capabilities Fe₃O₄-based Cu nano-architected electrodes for lithium-ion battery applications

Pierre-Louis Taberna, S. Mitra, Philippe Poizot, Patrice Simon, Jean-Marie Tarascon

► **To cite this version:**

Pierre-Louis Taberna, S. Mitra, Philippe Poizot, Patrice Simon, Jean-Marie Tarascon. High rate capabilities Fe₃O₄-based Cu nano-architected electrodes for lithium-ion battery applications. *Nature Materials*, 2006, 5, pp.567-573. 10.1038/nmat1672 . hal-03596243

HAL Id: hal-03596243

<https://hal.science/hal-03596243>

Submitted on 3 Mar 2022

HAL is a multi-disciplinary open access archive for the deposit and dissemination of scientific research documents, whether they are published or not. The documents may come from teaching and research institutions in France or abroad, or from public or private research centers.

L'archive ouverte pluridisciplinaire **HAL**, est destinée au dépôt et à la diffusion de documents scientifiques de niveau recherche, publiés ou non, émanant des établissements d'enseignement et de recherche français ou étrangers, des laboratoires publics ou privés.



Open Archive Toulouse Archive Ouverte (OATAO)

OATAO is an open access repository that collects the work of Toulouse researchers and makes it freely available over the web where possible.

This is an author-deposited version published in: <http://oatao.univ-toulouse.fr/>
Eprints ID : 2583

To link to this article :

URL : <http://dx.doi.org/10.1038/nmat1672>

To cite this version : Taberna, Pierre-Louis and Mitra , S. and Poizot, Philippe and Simon, Patrice and Tarascon, Jean-Marie (2006) [*High rate capabilities Fe₃O₄-based Cu nano-architected electrodes for lithium-ion battery applications.*](#)
Nature Materials, vol. 5 . pp. 567-573. ISSN 1476-1122

Any correspondence concerning this service should be sent to the repository administrator: staff-oatao@inp-toulouse.fr

High rate capabilities Fe₃O₄-based Cu nano-architected electrodes for lithium-ion battery applications

P. L. TABERNA¹, S. MITRA², P. POIZOT², P. SIMON^{1*} AND J.-M. TARASCON²

¹CIRIMAT-UMR 5085- Université Paul Sabatier, route de Narbonne, 31062 Toulouse Cedex 4, France

²LRCS-UMR 6007- Université de Picardie Jules Verne, 33 rue Saint-Leu, 80039 Amiens, France

*e-mail: simon@chimie.ups-tlse.fr

All battery technologies are known to suffer from kinetic problems linked to the solid-state diffusion of Li in intercalation electrodes, the conductivity of the electrolyte in some cases and the quality of interfaces. For Li-ion technology the latter effect is especially acute when conversion rather than intercalation electrodes are used. Nano-architected electrodes are usually suggested to enhance kinetics, although their realization is cumbersome. To tackle this issue for the conversion electrode material Fe₃O₄, we have used a two-step electrode design consisting of the electrochemically assisted template growth of Cu nanorods onto a current collector followed by electrochemical plating of Fe₃O₄. Using such electrodes, we demonstrate a factor of six improvement in power density over planar electrodes while maintaining the same total discharge time. The capacity at the 8C rate was 80% of the total capacity and was sustained over 100 cycles. The origin of the large hysteresis between charge and discharge, intrinsic to conversion reactions, is discussed and approaches to reduce it are proposed. We hope that such findings will help pave the way for the use of conversion reaction electrodes in future-generation Li-ion batteries.

Rechargeable Li-ion batteries now dominate the portable electronic market. These batteries are based on electrode reactions using classical intercalation reactions for which Li⁺ ions are inserted (or extracted) from an open host structure with a concomitant addition (or removal) of electrons. Although such batteries have gained commercial success, they fall short of satisfying needs for high power and/or capacities for applications such as power tools, electric vehicles or efficient use of renewable energies. The limitations to capacity are mainly due to the inability of the intrinsic capacity of such materials to reversibly incorporate more than one Li per 3d metal. Recently, conversion reactions of interstitial-free 3d metal oxide structures (CoO, CuO, NiO, and so on) with structures unsuitable for intercalation chemistry have nevertheless been shown to exhibit large, rechargeable capacities in cells with lithium^{1,2}. The specific capacities of these materials, which are potential candidates for the negative electrode, can be as high as 1,000 mA h g⁻¹ (that is, about three times those of commonly used graphitic carbons). This type of reaction now seems to be common and has been reported for nitrides, sulphides, fluorides and phosphides³⁻⁶. One drawback to date of conversion reactions is a marked hysteresis in voltage between charge and discharge. Therefore, we believe that to fully use these conversion reactions in practical cells it is imperative to reduce this hysteresis which currently limits both the energy efficiency and the power capabilities of batteries using conversion reactions.

The use of nanomaterials is a popular path to improve the rate capabilities of solid-state electrodes used in batteries because of the small diffusion lengths. The nanomaterials must then be elaborated into an electrode that maintains that diffusion length as well as providing electrical and mechanical contact through the strain imposed by the electrode reactions, accommodating structural strains that favour a longer calendar life. Soft-chemistry routes as well as template syntheses are among the most used methods to prepare non-self-supported nanometric materials⁷⁻¹⁰. Such approaches usually give nanosized materials (rods, wires, spheres, and so on) with enhanced electrochemical properties that need to be further processed into an electrode film. This comes with the risk of negating the gains in diffusion length

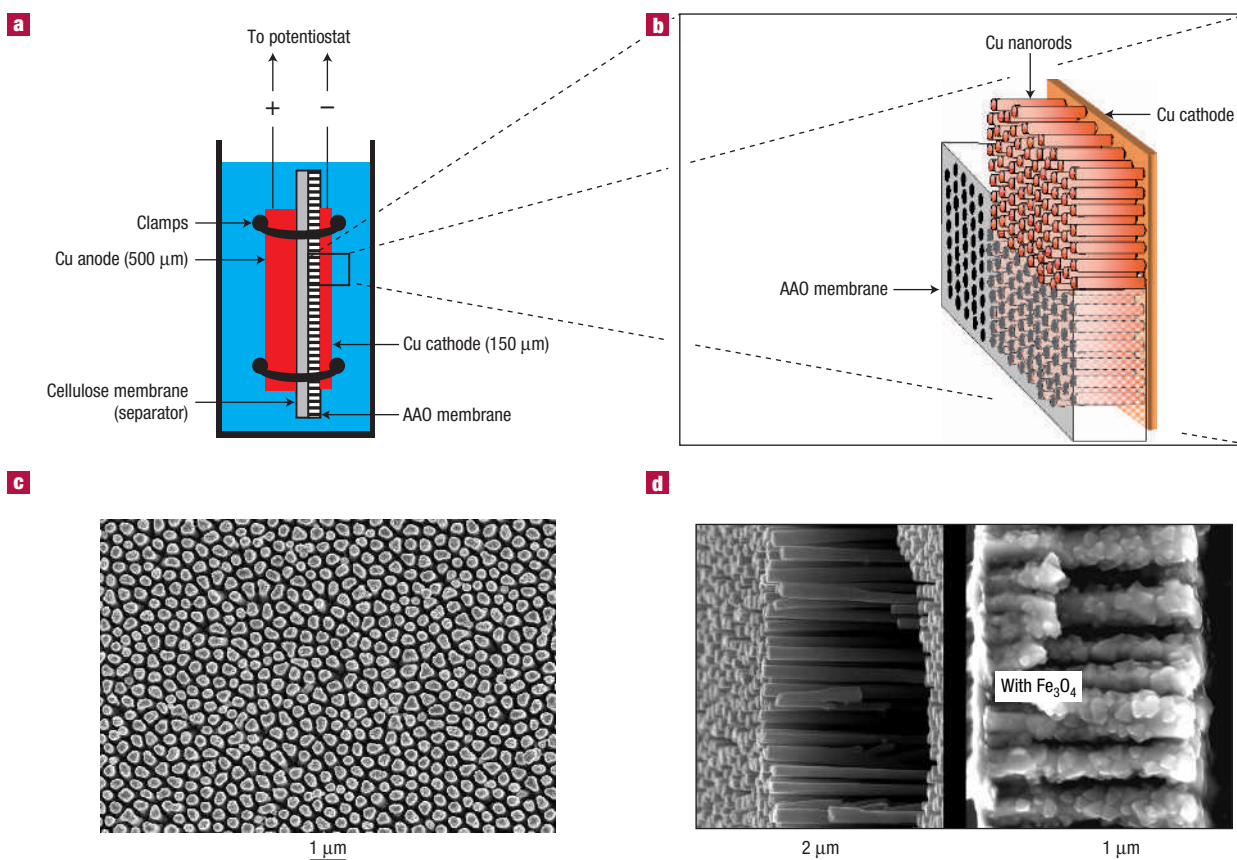


Figure 1 The electrochemical cell and the nanostructured current collector. **a**, Diagram of the electrochemical cell used for the template synthesis of the nanostructured Cu current collector. **b**, Diagram of the nanostructured current collector expected to be obtained at the end of the electrolysis, before and after removal of the AAO membrane. **c**, Top view of the Cu current collector obtained after electrolysis and membrane removal. **d**, Cross-sectional views of Cu-nanostructured current collector before (left) and after (right) Fe_3O_4 deposits.

and electronic conductivity associated with the reduced active-material particle size. There may also be new penalties arising from the addition of supplementary interfaces (that is, the current collector/active material and active material/active material). To preserve the benefits of electrochemistry at the nanoscale, and to achieve high rate capabilities, new electrode configurations were pioneered by Martin and co-workers. They consist of the direct elaboration of nano-architected electrodes by growing a nanostructured active insertion electrode material, either LiMn_2O_4 (refs 11,12), carbon¹³, V_2O_5 (refs 14,15), or more recently LiFePO_4 (ref. 16), onto a plane current collector thanks to a membrane acting as a template. Although quite attractive, this nano-architected electrode design cannot be blindly applied to elaborate 'efficient' conversion reaction-based electrodes of several micrometres thick bearing in mind that kinetic limitations are more acute for conversion reactions owing to the poor electronic/ionic conductivity of the $\text{M}_x\text{O}_y/\text{M}^0/\text{Li}_2\text{O}$ matrix. To promote better current collector/active material surface contacts, we grow an electrochemically active film onto a nano-architected current collector so that each particle of active material has its 'own' current collector. Along that line, insertion electrodes made of TiS_2 grown onto gold microtubular electrodes, made through a template-assisted synthesis, were successfully made¹⁷. However, that work was somewhat cumbersome with a complex elaboration process using several steps, and costly metals (Au).

Owing to the above obstacles, it seems that practical electrode manufacture would require a simpler electrode elaboration process compatible with the use of low-cost and high-performance materials, grown on noble metal-free current collectors. Keeping such needs in mind, we stuck to copper current collectors and chose Fe_3O_4 (magnetite) as a prototype conversion electrode material. Fe_3O_4 is an attractive material, being one of the cheapest common oxides, with very low toxicity¹⁸, and it is an environmentally friendly product (part of iron rust). It has been shown to act as a rechargeable conversion electrode material that reacts with eight Li per formula unit at a potential of 1.6 V versus Li^+/Li^0 (refs 19,20). Furthermore, this inverse spinel exhibits one of the highest electronic conductivities ($\sigma = 2 \times 10^4 \text{ S m}^{-1}$) of the simple oxides, which is only an order of magnitude less than the minimum metallic conductivity²¹.

Using the active material (Fe_3O_4) and current collector metal (Cu), we developed a new, but simple, two-step electrode fabrication process that differs from the previously reported procedures enlisting either template-assisted²²⁻²⁶ or costly micro- and photo-lithography techniques. Briefly, our process consists of growing a 3D array of copper nanorods onto a copper foil by electrodeposition through a porous anodic alumina membrane that is subsequently dissolved followed by electrodeposition of magnetite by cathodic reduction of a Fe(III) chelate precursor in alkaline solution. This process, discussed in greater detail below,

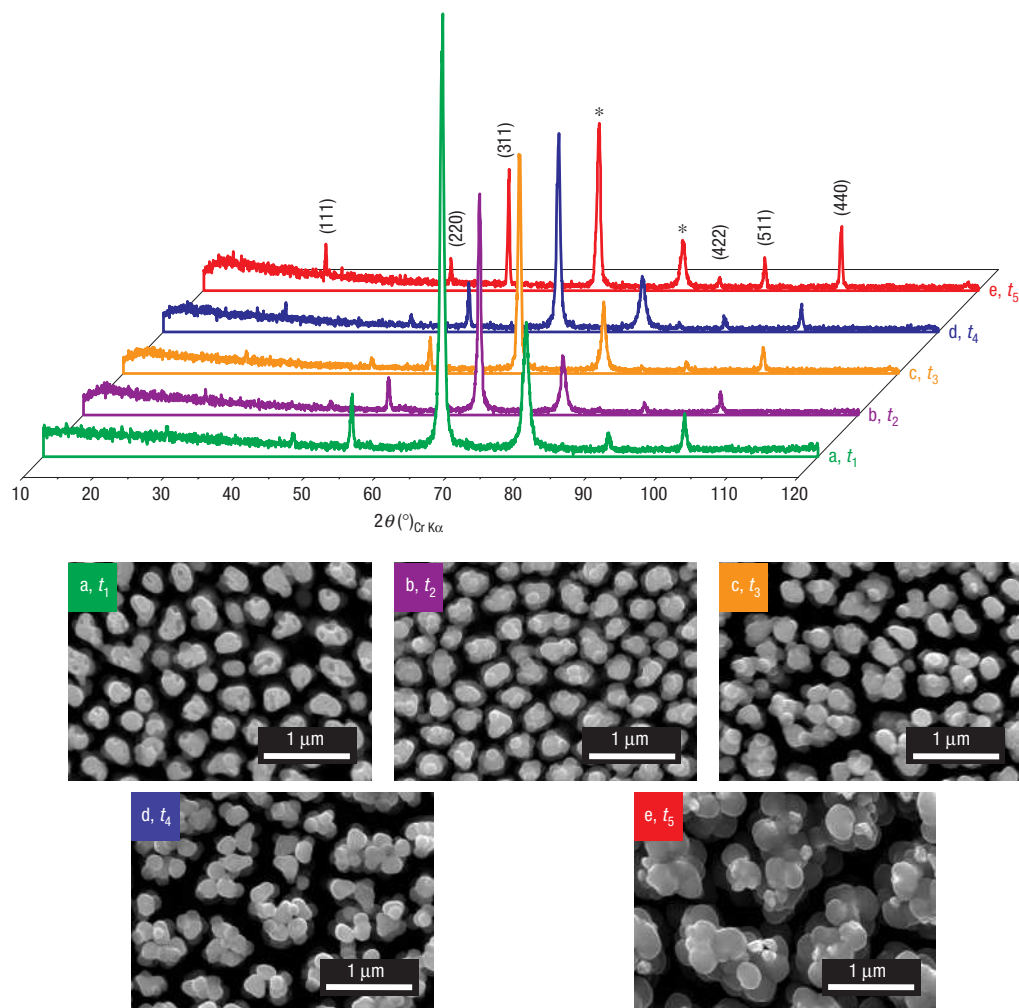


Figure 2 XRD patterns and scanning electron micrographs of as-prepared copper nanopillar Fe_3O_4 assemblies. X-ray diffraction patterns of Fe_3O_4 electrodeposited onto nano-architected current collectors for several deposition times at 50°C with an applied current density of -5 mA cm^{-2} ($t_1 = 120\text{ s}$, $t_2 = 150\text{ s}$, $t_3 = 180\text{ s}$, $t_4 = 230\text{ s}$ and $t_5 = 300\text{ s}$). (*) denotes the Bragg peaks of the copper substrate. The corresponding scanning electron micrographs are shown below.

affords low-cost rust-based nano-architected electrodes with high power capabilities and sustained rechargeability.

Our nano-architected Cu current collector was made by direct electrodeposition of copper into the pores of an anodized alumina oxide (AAO) membrane placed on top of a commercial copper foil which was polished and cleaned in ethanol before use (see the Methods section). To make high-quality electrodes we found it necessary to master, for the reasons described below, three experimental parameters: (i) the current distribution through the cell, (ii) the electrolyte feed into the pore of the membrane and (iii) the reaction kinetics limitations governed by the diffusion mass transfer.

Bearing in mind that the current distribution through the cell is the primary factor in controlling electrolysis, because it acts on the deposition kinetics²⁷ that can be limited by ohmic drops inside the cell, and charge or mass transfers, we designed our cell as shown in Fig. 1a to limit the ohmic drop across the cell, and thus to favour homogeneous copper deposits. We used a large (2.01 cm^2) and thin ($150\text{ }\mu\text{m}$) cathode copper current-collector foil together with a thick copper anode ($500\text{ }\mu\text{m}$) surrounded by $60\text{-}\mu\text{m}$ -thick Al_2O_3 (AAO) membranes with 200-nm pore sizes. A constant pressure

of 50 N cm^{-2} was applied to the stack by means of two stainless-steel clamps, thus reducing our ohmic drop across the cell down to $8\text{ }\Omega\text{ cm}^{-2}$.

Another key technological issue resulting from the introduction of the AAO membrane deals with its electrolyte loading/feeding and more specifically with means of ensuring a constant level of electrolyte inside the porous membrane kept under pressure between two metal foils. We found that this could not simply be achieved by dropping the clamped cell stack into the plating electrolyte. Therefore, the addition of a porous cellulose separator (Fig. 1a,b) between the anode and the top of the AAO membrane was found to be the most simple and elegant way to solve this key issue, while having little effect on the ohmic drop across the cell. In addition to preventing short circuits between anode and cathode, the capillary forces provided by the porous separator help maintain a continuous electrolyte flow from the bulk of the electrolyte to the porous alumina membrane, avoiding large Cu(II) concentration gradients inside the pores of the membrane. Such Cu(II) gradients would lead to diffusion-controlled copper electroplating and the possibility of dendritic or powdery Cu deposits or H_2 evolution. Finally, the separator accommodates the mechanical constraints of

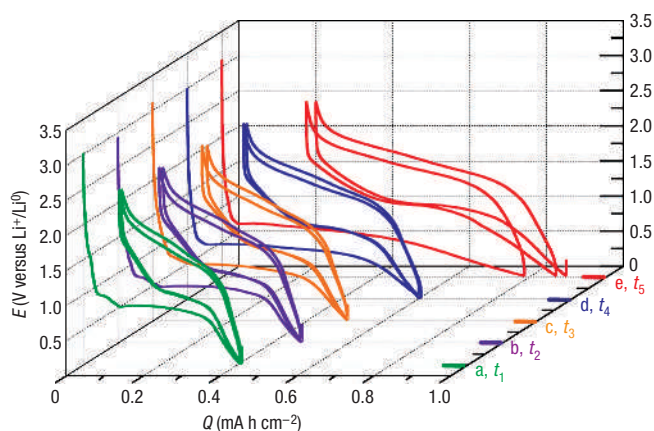


Figure 3 Potential-capacity profiles for the as-prepared copper-supported Fe_3O_4 deposits galvanostatically cycled at a rate of $1 \text{ Li}^+ / 2 \text{ h}$ versus Li. ($t_1 = 120 \text{ s}$, $t_2 = 150 \text{ s}$, $t_3 = 180 \text{ s}$, $t_4 = 230 \text{ s}$ and $t_5 = 300 \text{ s}$.) Note that the corresponding capacities were normalized towards the geometrical surface area of the commercial copper disk ($S = 2 \text{ cm}^2$).

the pressure applied to the stack that otherwise would lead to the destruction of the brittle AAO membrane.

Electrodeposition of Cu was carried out under a pulsed cathodic current, a technique applied for many years to the plating of metals or alloys²⁸ to avoid diffusion-limited deposition. We used a repeated sequence of 300 ms consisting of two steps. Initially, a low current density of -2 mA cm^{-2} is applied to the copper cathode for 250 ms. For the next 50 ms, the current density is increased to -30 mA cm^{-2} . These current densities were independently determined using a rotating-disk electrode. The pulse sequence was repeated for durations ranging from 30 to 60 min, depending on the type of Cu deposits desired. Herein we only discuss the results for a 30-min deposition time.

Figure 1c,d shows top and cross-section views of the Cu nanopillar current collectors in AAO after membrane removal. Obviously, the Cu surface is covered with uniformly distributed copper rods with diameters of 200 nm, defined by the pore size of the alumina membrane used, and of a uniform height of about 1,800 nm. Needless to say that by lowering the AAO pore size, we achieved 50 nm rods with the same uniformity both in width and height (not shown). Such a surprising uniformity distribution, approaching that of photolithography, validates the electrochemical approach described (that is, lower ohmic drop and homogeneous electrolyte flow).

The second keystone of our electrode preparation process deals with coating the Cu nanorod array with polycrystalline Fe_3O_4 . Again, electrochemical deposition emerges as a powerful technique as it also allows the direct fabrication of a perfect junction between metal and metal oxide, similar to a solder²⁹. On the basis of the work of Switzer and co-workers³⁰, we recently succeeded in making high rate electrodes by electrodeposition of polycrystalline Fe_3O_4 films on planar copper foil³¹. The optimized parameters ($T = 50 \text{ }^\circ\text{C}$, $t = 40 \text{ s}$, cathodic current density j of -5 mA cm^{-2}) previously established for the deposition on flat copper substrates failed to give good coverage on the Cu nanorod array owing to the large surface-area difference. Keeping all of the other parameters (T and j) constant, longer deposition times ranging from 120 to 300 s were applied to five pairs of Cu nanorod substrates. From each pair, one of the nano-architected current collectors was electrochemically tested versus Li, and the other was analysed by

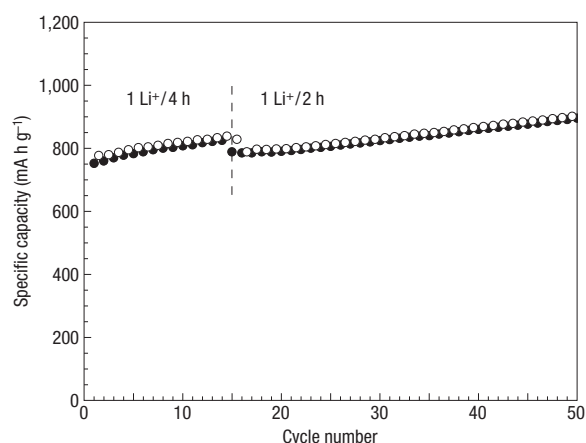


Figure 4 Capacity retention. The capacity retention of a Fe_3O_4 film electrodeposited onto nano-architected copper substrate for 150 s and cycled first at $1 \text{ Li}^+ / 4 \text{ h}$ for 15 cycles followed by a higher rate value of $1 \text{ Li}^+ / 2 \text{ h}$.

atomic absorption spectroscopy to determine the quantity of Fe_3O_4 deposited, because we found that the electrodeposition process did not exhibit 100% coulombic efficiency.

Figure 2 shows scanning electron micrographs and X-ray diffraction patterns of as-prepared copper nanopillar- Fe_3O_4 assemblies for five different deposition times. With the exception of the reflections owing to metallic copper, all Bragg peaks are consistent with those of the Fe_3O_4 phase (ICDD card No. 19-0629) with no preferred orientation. At the initial stage of the film growth, small and shapeless polycrystalline Fe_3O_4 grains cover the entire surface of the Cu nanorods. Then, with increasing electroplating time, the round islands at the tip of each nanorod become much more bulky, but no change is observed in the morphology of the grains. Note, for deposition times lower than 230 s, the copper nanorod was not fully covered with Fe_3O_4 , whereas a coalescence effect is observed for long deposition times (Fig. 2e). The resulting Cu nanorod electrodes, differentiated by their degree of Fe_3O_4 coverage, were characterized for their performance as electrodes in Li half cells which were cycled in a galvanostatic mode at a rate of 1 Li^+ per 2 h (Fig. 3). The potential versus capacity traces show that all cells behave similarly, showing the well-known signature of conversion reactions of transition-metal oxides^{1,2}. Systematically, the potential drops rapidly to reach a well-defined plateau below 1 V corresponding to the full reduction process of Fe_3O_4 into $\text{Fe}^0/\text{Li}_2\text{O}$ mixture followed by additional capacity. On cycling, the common hysteric profile is maintained, but these electrodes were found to show excellent capacity retention as shown in Fig. 4 for a 150-s deposition-time electrode. Capacity retention deteriorated faster for electrodes made using deposition times greater than 300 s; this is apparently due to the coalescence of the Fe_3O_4 particles, which blocks electrolyte accessibility to the space between the rods.

The self-supported $\text{Fe}_3\text{O}_4/\text{Cu}$ nano-architected electrodes were tested for their rate capability according to a protocol commonly used in the battery community, referred to as 'signature curve'³². Signature curves were collected on charge, using a cut-off potential of 2.5 V for cells stopped after their third discharge to 0.02 V at low current rate (1 Li in 2 h) to determine the full cell capacity (Q). Figure 5a shows the variation of the cell capacity as a function of the applied rate expressed in terms of C, with C being defined as the full use of the capacity (Q) in 1 h. For comparison, similar measurements were made on Li half cells

Table 1 Current density values used to plot the power capability of the nanostructured and planar Cu electrodes; values are given for the C rate determination.

t_1 (120 s)	0.314 mA cm ⁻² for C rate
t_2 (150 s)	0.363 mA cm ⁻² for C rate
t_3 (180 s)	0.366 mA cm ⁻² for C rate
t_4 (230 s)	0.450 mA cm ⁻² for C rate
t_5 (300 s)	0.655 mA cm ⁻² for C rate
40 s on planar Cu	0.0755 mA cm ⁻² for C rate

using, separately, (i) a plastic electrode film, made according to the Bellcore technology³³, containing 2 mg cm⁻² of commercial Fe₃O₄ powder (Aldrich) and (ii) a Fe₃O₄ film (referred to as 'Fe₃O₄-Cu' in Fig. 5a,b) grown on a planar Cu foil using the same electrodeposition technique and a 40-s deposit time. Table 1 lists the applied current densities for a 1C rate with respective nanostructured electrodes. Excellent rate capability is observed for all of the nano-architected electrodes compared with the Fe₃O₄ powder cell because they can recover 80% of their total capacity at an 8C rate, that is, in less than 7 min. Furthermore, we found that the cells retained full capacity for numerous cycles when cycling at high rates, indicative of the chemical/mechanical robustness of the electrodes. This was confirmed by a scanning electron microscopy observation of an electrode, after being cycled 100 times at a real C/2 rate (that is, 1 Li⁺/0.25 h), which revealed no peeling or other morphology changes of either the Fe₃O₄ or Cu nanorods (Fig. 5a, inset). Figure 5b stresses the benefit of having a nanostructured current collector as opposed to a planar one in terms of power density, because the current scales with the amount of Fe₃O₄ deposited allowing total discharge at comparable C rates. In short, the nano-architected electrode increases the power density by a factor of six.

The significance of these results is a demonstration that outstanding power densities from conversion reactions are possible by using nano-architected electrodes. Thus, they can be attractive to intercalation electrodes in Li-ion batteries, affording capacity gains (2.67 electrons per 3d-metal compared with ~1 for intercalation systems) without sacrificing power or cycle life. In the specific case of Fe₃O₄, there are also specific advantages of low cost and toxicity. However, excitement must still be tempered despite the present efforts aimed towards improving the electrode kinetics, because of the poor energy efficiency of conversion reactions which is manifested by a large charge/discharge potential difference (ΔE). This large polarization value is quite unusual and highlights a fundamental difference between conversion and insertion reactions, for which we do not have, to our knowledge, insertion materials showing the coexistence of large ΔE at low currents together with high rate capabilities. It is crucial to understand and improve the energy efficiency if conversion-based electrode materials are to go beyond a research curiosity.

To address energy efficiency, we first recall the factors affecting electrode reaction rates and, therefore, the electrode overpotential η . An overall electrode reaction basically enlists a sequence of reacting steps comprising charge-transfer and mass-transfer processes, adsorption, nucleation, and growth phenomena as well as chemical events, with its rate limited by any of the above. From a kinetic point of view, each step is characterized by a certain overpotential denoted η_{ct} for the charge-transfer overpotential, η_{mt} for the mass-transfer overpotential, and so on³⁴, so that the total electrode potential can be considered as the sum of each contribution (that is, $\eta = \eta_{ct} + \eta_{mt} + \dots$), and can be experimentally determined from the following general relation $\eta = E_{meas} - E_{eq}$, where E_{eq} is the equilibrium potential and E_{meas}

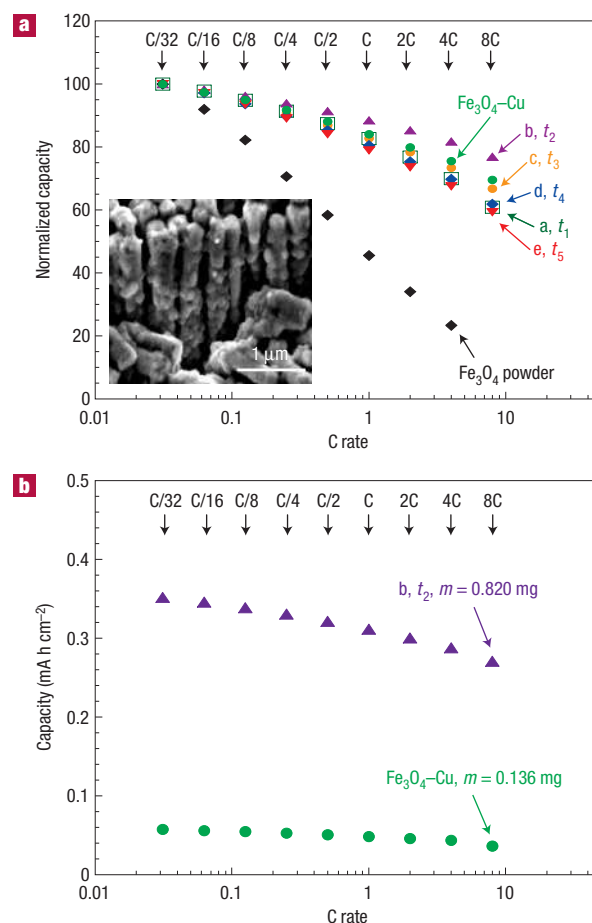


Figure 5 Rate capability. **a**, Rate capability plots for the five Fe₃O₄ deposits on Cu nanostructured electrodes, compared with (1) a Fe₃O₄ deposit denoted 'Fe₃O₄-Cu' grown on a planar Cu foil electrode using the same experimental conditions as the nanostructured deposits (see ref. 31) and (2) a 1 cm² plastic positive electrode film based on commercial Fe₃O₄ powders. The electrode film was cast and processed using a procedure reported previously³³ from a mixture containing 60 wt% Fe₃O₄ powder, 22 wt% SP carbon black (MMM Carbon, Belgium), and 18 wt% poly(vinylidene)fluoride co-hexafluoropropylene copolymer binder. The charge data were obtained once the cell's third discharge was completed, by carrying out what is called a 'signature curve' test, according to ref. 32 (also see the Methods section). Inset: scanning electron micrograph of a copper-supported Fe₃O₄ deposit cycled galvanostatically 100 times at a high rate (that is, 1 Li⁺/0.3 h) showing the good stability of the electrode although a very small amount of active material (lowest deposition time, $t_1 = 120$ s). **b**, For comparison, the normalized capacity (mA h cm⁻² of geometrical surface area) is plotted versus rate for our optimized Fe₃O₄-based Cu-nanostructured electrode and a Fe₃O₄-based Cu planar electrode made according to ref. 31; that is, using the same Fe₃O₄ electrodeposition technique as reported herein.

is the experimentally measured potential (against an ideal non-polarizable electrode). At this stage, it is virtually impossible to determine the physical origin of the measured η in our cells so as to spot the rate-determining step. Galvanostatic-intermittent-titration-technique-type measurements³⁵, which combine transient and steady-state measurements, are a common way to determine the equilibrium potentials and obviously η values. However, we find that very long relaxation periods are needed to reach equilibrium, indicative of the existence of long-lasting chemical

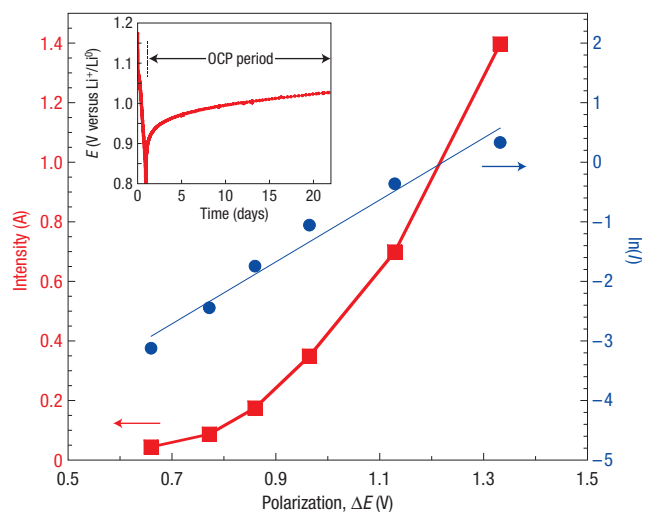


Figure 6 $\ln(I_{\text{applied}})$ versus ΔE and I_{applied} versus ΔE . Polarization values were extracted from the middle of the sloppy plateaux of a Li half cell cycled at different C rates (ranging from C/32 (1 Li⁺/4 h) to C/2 (1 Li⁺/0.25 h)) and plotted according to a Tafel plot ($\ln(I_{\text{applied}})$ versus ΔE) and I_{applied} versus ΔE . Inset: extra-long relaxation period after 5 h under reducing current.

gradients, and therefore poor transport kinetics in our conversion electrodes. This is consistent with the results of Novák on CuO cells claiming that a 2-month period was necessary for a CuO electrode to reach a steady equilibrium potential after applying a current pulse³⁶. Owing to the difficulties in reaching equilibrium, we directly use the cell polarization values versus Li (that is, the charge/discharge hysteresis) denoted ΔE and defined as $\Delta E = E_{\text{anodic}} - E_{\text{cathodic}} = \eta_{\text{anodic}} - \eta_{\text{cathodic}}$ to bypass the knowledge of E_{eq} and indirectly determine η , if we consider the Li⁺/Li⁰ system as a non-polarizable electrode. By assuming, in a first approximation, an equivalent overpotential amplitude both under positive and negative currents for a fixed extent of reaction, η becomes equal to $(1/2)\Delta E$. Thus, the variations in ΔE as function of rate can be studied.

To carry out this study, another Li half cell using a self-supported Cu-nanorod Fe₃O₄ electrode as the positive electrode was galvanostatically cycled at rates ranging from C/32 (1 Li⁺/4 h) to C/2 (1 Li⁺/0.25 h) and the polarization values were extracted from the middle of the sloppy plateaux. Interestingly, a conventional polarization plot (I_{applied} or C versus ΔE) did not fit well with a linear relation, disclaiming an ohmic behaviour of the conversion reaction at a relatively low rate. However, to our surprise, a quasi-linear correlation was noted (Fig. 6) when the data was plotted according to a Tafel plot ($\ln I_{\text{applied}}$ versus ΔE). Therefore, the electrochemical system behaves as an impedance with an activation step and not as a pure resistance. As the charge transfer process is the rate-determining step for conversion reactions as deduced by electrochemical impedance spectroscopy³⁷, which has revealed a Randles-like behaviour (that is, the presence of one small semicircle plus a Warburg impedance on the Nyquist plot), the Tafel-like behaviour is strongly indicative that the kinetic barrier could be nested in an Arrhenius-type limiting kinetic. Chemically speaking, as conversion reactions enlist three solid-state components during the charge/discharge processes, it is easily conceivable that the reaction is governed by mass transfer through grain boundaries. In this respect, a comprehensive comparison is easily made if we consider solid-state double decomposition

reactions, for which large activation energies are measured and found to decrease with decreasing reagent particle size³⁸. Thus, although we have a high rate capacity electrode, the activation barrier to trigger the oxidation and reduction reactions is still high and quite similar to a conventional powder-based conversion electrode. So, whatever the initial configuration of the conversion electrode (powder-based or nano-architected) the activation barrier seems to be directly linked to the size and the nature of the uniformly dispersed nanocomposite electrode produced *in situ* after the first discharge.

Finally, this scenario is also consistent with previous reports showing a decrease in ΔE when oxides and phosphides are used instead of Co-based binary fluorides because the nanometric matrix is chemically different when changing the anion (Li⁺ as well as Mⁿ⁺ or X^{m-} can be more mobile). Naively, temperature could be thought of as the easiest way to trigger the energetic barrier, and thus to realize conversion reactions with low polarization. As previously mentioned³, to bypass this limitation inherent to this peculiar heterogeneous electrochemical process, the second-kind electrode concept, where only two solid phases are involved, should be considered. Relevant examples are known to the field of batteries, such as ZEBRA batteries, which use liquid salt (NaAlCl₄) and metallic nickel as the raw material³⁹, or the cadmium-based electrode which, for a long time, has commonly been used as the negative electrode in Ni–Cd cells. In the former case, the half reaction can be written as $\text{Cd}(\text{OH})_{2(\text{s})} + 2\text{e}^- \rightleftharpoons \text{Cd}^0 + 2\text{OH}^-_{(\text{aq})}$, which is quite similar to the conversion reactions based on oxides except that the oxygen vehicles are soluble rather than solid species.

Advances in these directions may emerge with further chemistry considerations aiming towards the identification/design of the ‘magic’ soluble salt in non-aqueous media required when using Li. Preliminary attempts towards such a direction are in progress. Finally, we recognize that this is only one electrode and a battery must have two electrodes. The high-rate LiMn_{0.5}Ni_{0.5}O₂ positive material recently reported by Ceder and co-workers⁴⁰ would provide a 2 V cell.

METHODS

FABRICATION OF COPPER NANOPILLAR ARRAYS

Arrays of highly perpendicular copper nanopillars on copper disk substrate (2 cm², 150- μm thick, 99.9% Cu, Goodfellow) were fabricated by cathodic electrodeposition from an electrolytic bath consisting of CuSO₄ · 5H₂O 100 g L⁻¹, (NH₄)₂SO₄ (Acros Organics) 20 g L⁻¹ and diethyl-tri-amine (DETA, Acros Organics) 80 mL L⁻¹, inside the pores of an alumina oxide membrane (AAO, Whatman, Anodisc 47, reference 6809 5022), with an Arbin BT2000 potentiostat/galvanostat. The membrane was 60- μm thick, with a maximum porosity between 50 and 65%, a diameter of about 47 mm, and a pore density of 10¹⁰ cm⁻². Before using the cathode foil, it was mechanically polished, first with SiC paper then with 6, 3, 1 and 0.25- μm alumina slurry. After being rinsed with deionized water and ultrasonically cleaned in ethanol, the copper cathode was assembled in front of a copper anode. The outer parts of the copper anode and cathode were protected from dissolution or deposition by isolating adhesive film. The cellulose paper separator (Whatman, reference 1441-055) was 215- μm thick, with a weight of 85 m² g⁻¹ and a mean porous density of 20 μm . The resulting two-electrode stack was kept under a constant diameter by using two stainless-steel clamps during the deposition process.

Electrochemical Cu deposit was achieved using a pulsed cathodic current technique. This technique differs from the standard constant current deposit in that the current profile changes with time. The pulsed current deposition technique is generally used to limit the active-species depreciation in complex-geometry electrochemical cells. Here, a two-step profile is used:

Step 1: a cathodic current pulse of -2 mA cm^{-2} for 250 ms

Step 2: a cathodic current pulse of -30 mA cm^{-2} for 50 ms.

After deposition, the two-electrode stack is removed from the solution under current, and the cell is dismantled. The cathode is soaked in hot alkaline solution (pH = 14, 80 °C) to remove the AAO membrane, then in an acidic

copper sulphate bath (pH = 1, 25 °C) to dissolve the surface copper oxide. Current collectors are then stored into a glove box under a 6.0 argon atmosphere preventing them from further oxidation.

Cu-NANOPILLARS-Fe₃O₄ ASSEMBLY AND CHARACTERIZATION

Copper nanopillars were covered with Fe₃O₄ by means of an electrodeposition process from an alkaline aqueous solution (pH = 12.3) consisting of 2 M NaOH, 0.09 M Fe₂(SO₄)₃ · 5H₂O (Alfa Aesar) complexed with 0.1 M tri-ethanol-amine (Acros Organics)^{30,31}. The magnetite coating was produced under stirring at a constant current density ($j = -5 \text{ mA cm}^{-2}$) using a three-electrode cell set-up maintained at a fixed temperature of 50 °C. Copper substrate containing copper nanopillars acted as the working electrode, whereas a coil of platinum wire served as the auxiliary electrode. All potentials were quoted against an HgO/Hg⁰ reference electrode. The electrodeposits were carried out for several deposition times using a VMP Potentiostat/Galvanostat (Princeton Applied Research) operating in a galvanostatic mode. All electrode assemblies were systematically examined by X-ray diffraction (Inel CPS 120, Cr K α) and scanning electron microscopy (QUANTA 200 F). The amount of deposited Fe₃O₄ was determined by a preliminary study using the atomic absorption spectroscopy (Perkin Elmer Analyst 300, $\lambda_{\text{Fe}} = 248.3 \text{ nm}$) as the analytical tool.

ELECTROCHEMICAL BEHAVIOUR WITH LITHIUM

Coin-type cells were assembled in an argon-filled dry box using the copper nanopillar-Fe₃O₄ assembly as the positive electrode and the Li metal as the negative electrode. Both positive and negative electrodes were electronically separated by a Whatman GF/D borosilicate glass-fibre sheet saturated with 1 M LiPF₆ electrolyte solution (in EC:DMC/1:1 in mass ratio) purchased from Merck. Unless it is stated otherwise, the cells were first galvanostatically cycled between 2.5 and 0.02 V for two-and-a-half cycles at a rate of 1 electron exchanged per Fe₃O₄ formula unit in 2 h (1 Li⁺/2 h). From the as-obtained electrochemical data, the real full delivered capacity of the positive electrode (denoted Q, mA h) was calculated for the entire examined cell once the cell's third discharge, carried out in galvanostatic mode at low current density (1 Li⁺/2 h rate), was complete. It is then possible to determine the rate capability aptitude of our copper-supported Fe₃O₄ deposits using a 'signature curve'³² according to the following conditions.

As an example, for the cell based on our t₂ samples, we used a charge current of $j_1 = 2.904 \text{ mA cm}^{-2}$ (8C) to a charge cut-off voltage of 2.5 V versus Li⁺/Li. When the battery reaches 2.5 V, the cell has delivered the capacity Q_{p,1} (with Q_{p,1} = $j_1 \times t_{p,1}$) and it is automatically placed in open-circuit potential for 300 s ($j = 0$). Afterwards, the same sequence is repeated seven more times with the charging current always being reduced by a factor 2 during subsequent steps (that is, $j_2 = j_1/2$ and so on). The capacity versus rate curve is then obtained by cumulating the measured capacity for each step (that is, Q_{p,1}; j₁; Q_{p,1} + Q_{p,2}; j₂; Q_{p,1} + Q_{p,2} + Q_{p,3}; j₃) that represents the total cell capacity delivered at current density values j₁, j₂ and j₃, respectively.

References

- Poizot, P., Laruelle, S., Grugeon, S., Dupont, L. & Tarascon, J.-M. Nano-sized transition metal oxides as negative electrode material for lithium-ion batteries. *Nature* **407**, 496–499 (2000).
- Tarascon, J.-M., Grugeon, S., Laruelle, S., Larcher, D. & Poizot, P. in *Lithium Batteries—Science and Technology* (eds Nazri, G. A. & Pistoia, G.) Ch. 7 (Kluwer Academic, Boston, 2003).
- Poizot, P., Laruelle, S., Grugeon, S. & Tarascon, J.-M. Rationalization of the low-potential reactivity of 3d-metal-based inorganic compounds toward Li. *J. Electrochem. Soc.* **149**, A1212–A1217 (2002).
- Pereira, N., Klein, L. C. & Amatucci, G. G. The electrochemistry of Zn₃N₂ and LiZnN. A lithium reaction mechanism for metal nitride electrodes. *J. Electrochem. Soc.* **149**, A262–A2717 (2002).
- Pralong, V., Souza, D. C. S., Leung, K. T. & Nazar, L. F. The mechanism of reversible lithium uptake in CoP₂ at low potential: role of the anion. *Electrochem. Commun.* **4**, 516–520 (2002).
- Li, H., Balaya, P. & Maier, J. Li-storage via heterogeneous reaction in selected binary metal fluorides and oxides. *J. Electrochem. Soc.* **151**, A1878–A1885 (2004).

- Whitehead, A. H., Elliott, J. M. & Owen, J. R. Nanostructured tin for use as a negative electrode material in Li-ion. *J. Power Sources* **81–82**, 33–38 (1999).
- Kavan, L. & Grätzel, M. Facile synthesis of nanocrystalline Li₄Ti₅O₁₂ (spinel) exhibiting fast Li insertion. *Electrochem. Solid-State Lett.* **5**, A39–A42 (2002).
- Dewan, C. & Teeters, D. Vanadia xerogel nanocathodes used in lithium microbatteries. *J. Power Sources* **119–121**, 310–315 (2003).
- Yan, H. et al. Colloidal-crystal-templated synthesis of ordered macroporous electrode materials for Lithium secondary batteries. *J. Electrochem. Soc.* **150**, A1102–A1107 (2003).
- Nishizawa, M., Mukai, K., Kuwabata, S., Martin, C. R. & Yoneyama, H. Template synthesis of polypyrrole-coated spinel LiMn₂O₄ nanotubes and their properties as cathode active materials for lithium batteries. *J. Electrochem. Soc.* **144**, 1923–1927 (1997).
- Li, N., Patrissi, C. J. & Martin, C. R. Rate capabilities of nanostructured LiMn₂O₄ electrodes in aqueous electrolyte. *J. Electrochem. Soc.* **147**, 2044–2049 (2000).
- Li, N., Mitchell, D. T., Lee, K.-P. & Martin, C. R. A nanostructured honeycomb carbon anode. *J. Electrochem. Soc.* **150**, A979–A984 (2003).
- Patrissi, C. J. & Martin, C. R. Sol-gel-based template synthesis and Li-insertion rate performance of nanostructured vanadium pentoxide. *J. Electrochem. Soc.* **146**, 3176–3180 (1999).
- Patrissi, C. J. & Martin, C. R. Improving the volumetric energy densities of nanostructured V₂O₅ electrodes prepared using the template method. *J. Electrochem. Soc.* **148**, A1247–A1253 (2001).
- Croce, F., Sides, C. R., Young, V. Y., Martin, C. R. & Scrosatti, B. A high-rate, nanocomposite LiFePO₄/carbon cathode. *Electrochem. Solid-State Lett.* **8**, A484–A487 (2005).
- Che, G., Jirage, K. B., Fisher, E. R., Martin, C. R. & Yoneyama, H. Chemical-vapor deposition-based template synthesis of microtubular TiS₂ battery electrodes. *J. Electrochem. Soc.* **144**, 4296–4302 (1997).
- Hussain, S. M., Hess, K. L., Gearhart, J. M., Geiss, K. T. & Schlager, J. J. In vitro toxicity of nanoparticles in BRL 3A rat liver cells. *Toxicol. in Vitro* **19**, 975–983 (2005).
- Thackeray, M. M. & Coetzer, J. A preliminary investigation of the electrochemical performance of α -Fe₂O₃ and Fe₃O₄ cathodes in high-temperature cells. *Mater. Res. Bull.* **16**, 591–597 (1981).
- Thackeray, M. M., David, W. I. F. & Goodenough, J. B. Structural characterization of the lithiated iron oxides Li_xFe₂O₄ and Li_xFe₃O₄ (0 < x < 2). *Mater. Res. Bull.* **17**, 785–793 (1982).
- Coej, J. M. D., Berkowitz, A. E., Balcells, L., Putris, F. E. & Parker, F. T. Magnetoresistance of magnetite. *Appl. Phys. Lett.* **72**, 734–736 (1998).
- Martin, C. R. Membrane-based synthesis of nanomaterials. *Chem. Mater.* **8**, 1739–1746 (1996).
- Dobrev, D., Vetter, J. & Angert, N. Electrochemical preparation of metal microstructures on large areas of etched ion track membranes. *Nucl. Instrum. Methods B* **149**, 207–212 (1999).
- Konishi, Y. et al. Electrodeposition of Cu nanowire arrays with a template. *J. Electroanal. Chem.* **559**, 149–153 (2003).
- Leopold, S. et al. Electrochemical deposition of cylindrical Cu/Cu₂O microstructures. *Electrochim. Acta* **47**, 4393–4397 (2002).
- Valizadeh, S., George, J. M., Leisner, P. & Hultman, L. Electrochemical synthesis of Ag/Co multilayered nanowires in porous polycarbonate membranes. *Thin Solid Films* **402**, 262–271 (2002).
- Wendt, H. & Kreysa, G. *Electrochemical Engineering* (Springer, Berlin Heidelberg, 1999).
- Ueda, M. et al. Double-pulse technique as an electrochemical tool for controlling the preparation of metallic nanoparticles. *Electrochim. Acta* **48**, 377–386 (2002).
- Oh, J., Tak, Y. & Lee, J. Electrochemically deposited nanocolumnar junctions of Cu₂O and ZnO on Ni nanowires. *Electrochem. Solid-State Lett.* **8**, C81–C84 (2005).
- Kothari, H. M. et al. Electrochemical deposition and characterization of Fe₃O₄ films produced by the reduction of Fe(III)-triethanolamine. *J. Mater. Res.* **21**, 293–301 (2006).
- Mitra, S., Poizot, P., Finke, A. & Tarascon, J.-M. Growth and electrochemical characterization vs. Li of Fe₂O₃ electrodes made by electrodeposition. *Adv. Funct. Mater.* in the press.
- Doyle, M., Newman, J. & Reimers, J. A quick method of measuring the capacity versus discharge rate for a dual lithium-ion insertion cell undergoing cycling. *J. Power Sources* **52**, 211–216 (1994).
- Tarascon, J.-M., Gozdz, A. S., Schumtz, C., Shokoohi, F. & Warren, P. C. Performance of Bellcore's plastic rechargeable Li-ion batteries. *Solid State Ion.* **86–88**, 49–54 (1996).
- Bard, J. A. & Faulkner, L. R. *Electrochemical Methods* (Wiley, New York, 2001).
- Weppner, W. & Huggins, R. A. Determination of the kinetic parameters of mixed-conducting electrodes and application to the system Li₂Sb. *J. Electrochem. Soc.* **124**, 1569–1578 (1977).
- Novák, P. CuO cathode in lithium cells—II. Reduction mechanism of CuO. *Electrochim. Acta* **30**, 1687–1692 (1985).
- Kang, Y.-M. et al. A study on the charge-discharge mechanism of Co₃O₄ as an anode for the Li ion secondary battery. *Electrochim. Acta* **50**, 3667–3673 (2005).
- Kutty, T. R. N. & Murthy, A. R. V. Solid state reaction between urea nitrate and tricalcium phosphate. Mechanistic study. *Indian J. Technol.* **12**, 447–450 (1974).
- Dustmann, C.-H. Advances in ZEBRA batteries. *J. Power Sources* **127**, 85–92 (2004).
- Kang, K., Meng, Y. S., Bréger, J., Grey, C. P. & Ceder, G. Electrodes with high power and high capacity for rechargeable lithium batteries. *Science* **311**, 977 (2006).

Acknowledgements

The authors express their sincere gratitude to D. Murphy for helpful comments and discussions on this manuscript and the European Network of Excellence 'ALISTORE' for providing the ground scientific discussions to ignite such a study. The authors are deeply grateful to the EU for co-financing ALISTORE.